Molecular Therapy
Methods & Clinical Development
Original Article

Preclinical evaluation of the efficacy and safety of AAV1-hOTOF in mice and nonhuman primates

Longlong Zhang,[1,2,3,6] Hui Wang,[1,2,3,6] Mengzhao Xun,[1,2,3,6] Honghai Tang,[1,2,3,6] Jinghan Wang,[1,2,3] Jun Lv,[1,2,3] Biyun Zhu,[1,2,3] Yuxin Chen,[1,2,3] Daqi Wang,[1,2,3] Shaowei Hu,[1,2,3] Ziwen Gao,[1,2,3] Jianping Liu,[1,2,3] Zheng-Yi Chen,[4,5] Bing Chen,[1,2,3] Huawei Li,[1,2,3] and Yilai Shu[1,2,3]

[1]ENT Institute and Otorhinolaryngology Department of Eye & ENT Hospital, State Key Laboratory of Medical Neurobiology and MOE Frontiers Center for Brain Science, Fudan University, Shanghai 200031, China; [2]Institutes of Biomedical Science, Fudan University, Shanghai 200032, China; [3]NHC Key Laboratory of Hearing Medicine, Fudan University, Shanghai 200031, China; [4]Department of Otolaryngology-Head and Neck Surgery, Graduate Program in Speech and Hearing Bioscience and Technology and Program in Neuroscience, Harvard Medical School, Boston, MA 02115, USA; [5]Eaton-Peabody Laboratory, Massachusetts Eye and Ear, 243 Charles Street, Boston, MA 02114, USA

Pathogenic mutations in the *OTOF* gene cause autosomal recessive hearing loss (DFNB9), one of the most common forms of auditory neuropathy. There is no biological treatment for DFNB9. Here, we designed an *OTOF* gene therapy agent by dual-adeno-associated virus 1 (AAV1) carrying human *OTOF* coding sequences with the expression driven by the hair cell–specific promoter *Myo15*, AAV1-hOTOF. To develop a clinical application of AAV1-hOTOF gene therapy, we evaluated its efficacy and safety in animal models using pharmacodynamics, behavior, and histopathology. AAV1-hOTOF inner ear delivery significantly improved hearing in *Otof*$^{-/-}$ mice without affecting normal hearing in wild-type mice. AAV1 was predominately distributed to the cochlea, although it was detected in other organs such as the CNS and the liver, and no obvious toxic effects of AAV1-hOTOF were observed in mice. To further evaluate the safety of *Myo15* promoter-driven AAV1-transgene, AAV1-GFP was delivered into the inner ear of *Macaca fascicularis* via the round window membrane. AAV1-GFP transduced 60%–94% of the inner hair cells along the cochlear turns. AAV1-GFP was detected in isolated organs and no significant adverse effects were detected. These results suggest that AAV1-hOTOF is well tolerated and effective in animals, providing critical support for its clinical translation.

INTRODUCTION

Disabling hearing loss is a common sensory deficit, with ~466 million people affected worldwide,[1] and genetic defects account for 60% of congenital hearing loss.[2,3] To date, clinical therapeutic strategies rely mainly on hearing aids or cochlear implantation to alleviate genetic hearing loss.[4–6] However, these approaches are limited by their sensitivity and their ability to perceive musical rhythm and natural sounds, especially in noisy environments.[7–13] Thus, there is an urgent need to explore novel treatment strategies for hereditary hearing loss, and with technical developments in the delivery and genome editing tools, etiology-based gene therapy has emerged as a promising strategy for hereditary hearing loss.[14–17]

DFNB9 is a form of congenital profound deafness due to mutations in the *OTOF* gene and accounts for 2%–8% of hereditary deafness.[15,18–21] Over 200 pathogenic mutations have been identified in the *OTOF* gene.[22,23] Pathogenic mutations in *OTOF* gene disrupt otoferlin function in the inner hair cells (IHCs),[24] leading to almost completely abolished exocytosis function of IHCs and resulting in sensorineural hearing loss.[25,26]

Due to the large size of *OTOF* cDNA (~6 kb), gene replacement strategies based on the nucleic acid or protein recombination of dual-adeno-associated virus (AAV) rescued hearing loss in the *Otof*$^{-/-}$ mouse models.[15–17] However, these strategies still lack the safety evaluations required to advance to the clinical stage. In previous studies, the delivery tools (AAVs) used ubiquitous promoters such as cytomegalovirus and chicken β-actin promoter (CAG) lacked target specificity for HCs in the cochlea,[15–17] which may result in *OTOF* expression in nonhair cells, which may lead to adverse effects.[27,28] As a

Received 25 August 2023; accepted 7 November 2023;
https://doi.org/10.1016/j.omtm.2023.101154.

[6]These authors contributed equally

Correspondence: Bing Chen, ENT Institute and Otorhinolaryngology Department of Eye & ENT Hospital, State Key Laboratory of Medical Neurobiology and MOE Frontiers Center for Brain Science, Fudan University, Shanghai 200031, China.
E-mail: bingchen@fudan.edu.cn
Correspondence: Huawei Li, ENT Institute and Otorhinolaryngology Department of Eye & ENT Hospital, State Key Laboratory of Medical Neurobiology and MOE Frontiers Center for Brain Science, Fudan University, Shanghai 200031, China.
E-mail: hwli@shmu.edu.cn
Correspondence: Yilai Shu, ENT Institute and Otorhinolaryngology Department of Eye & ENT Hospital, State Key Laboratory of Medical Neurobiology and MOE Frontiers Center for Brain Science, Fudan University, Shanghai 200031, China.
E-mail: yilai_shu@fudan.edu.cn

result, it is unclear whether the previous *OTOF* treatments pose potential safety risks. To minimize the potential risk, a cell-type-specific promoter is required to restrict the *OTOF* expression to hair cells that are physiologically relevant.

We designed a treatment system, AAV1-hOTOF (human *OTOF*), that consists of the HC-specific promoter *Myo15* and the human *OTOF* coding sequences (CDSs) mediated by AAV1, which has been approved to treat multiple human diseases.[29–33] We report the assessment of the efficacy and safety of the AAV1-transgene driven by the *Myo15* promoter in mice and nonhuman primates (NHPs) through pharmacodynamics measurements, behavioral tests, and histopathology analysis. This study provides valuable efficacy and safety data for conducting clinical trials of AAV1-hOTOF.

RESULTS

Hearing in *Otof*$^{-/-}$ mice was rescued after AAV1-hOTOF injection

To promote otoferlin gene therapy for clinical application, we selected a relatively safe AAV1 as delivery tool, and confirmed that AAV1 transfected IHCs effectively (Figures S1A and S1B), consistent with previous reports.[34–36] Given that the length of *OTOF* CDSs exceeds the cargo capacity of AAV vectors, dual-AAV strategy was explored to successfully overcome the size limitation,[15–17] including *trans*-splicing (TS) and hybrid strategies.[37] In the TS strategy, the fragment from splice donor (SD) to splice acceptor (SA) is spliced out by intracellular spliceosome after recombination and transcription of transgene, which generates a mature mRNA and translates functional protein.[38,39] The principle of the hybrid strategy is similar to that of the TS strategy, except that an additional homologous arm (e.g., alkaline phosphatase (AP) or the F1 phage [AK], a highly recombinogenic region) is added between the SD and SA of transgene.[39–41] To increase recombinational efficiency between the dual-AAVs, the AK/AP was placed downstream of the SD signal in the 5′ half-vector and upstream of the SA signal in the 3′ half-vector (Figure S2A). Next, we screened out an ideal recombination strategy for *OTOF* gene therapy at the nucleic acid level by western blot and auditory tests (Figures S2B and S2C), indicating that the AK strategy outperformed other two strategies (TS and AP).[39] For this, we used a dual-AAV1-Hyb (AK) approach in which the human *OTOF* CDS was driven by the HC-specific promoter *Myo15*, called AAV1-hOTOF.

To further systematically evaluate the efficacy of AAV1-hOTOF in treating *Otof* $^{-/-}$ mice, we injected newborn mice via the round window membrane (RWM) at postnatal day 0–2 (P0–P2). As shown in Figure 1A, the untreated *Otof* $^{-/-}$ mice were profoundly deaf, with no identifiable auditory brainstem response (ABR) waves elicited by the maximum 90-dB sound pressure level (SPL), whereas the AAV1-hOTOF injected ear of *Otof* $^{-/-}$ mice displayed distinct ABR waves. To further explore the relationship between dose and efficacy, four doses were tested, including the high-dose group (6×10^{10} viral genomes (vg)/cochlea), the intermediate- to high-dose group (3×10^{10} vg/cochlea), the intermediate-dose group (1.5×10^{10} vg/cochlea), and the low-dose group (7.5×10^{9} vg/cochlea). ABRs in response to click and tone-burst stimuli were recorded 1 month after injection. In the injected ears, the click ABR thresholds were significantly rescued in the high-dose group (60.83 ± 4.17 dB), the intermediate- to high-dose group (62.92 ± 3.72 dB), and the intermediate-dose group (65.42 ± 2.08 dB), whereas the low-dose group only showed minimal hearing recovery (83.13 ± 5.34 dB) (Figure 1B). The ABR thresholds in response to tone-burst stimuli also showed a trend toward better efficacy from low dose to high dose, suggesting a possible dose-dependent effect. The ABR threshold in the high-dose group was not different compared with the intermediate- to high-dose group at all frequencies. However, there were significant differences between high- and intermediate-dose groups at 4 and 32 kHz ($p < 0.01$ and $p < 0.05$, respectively), and there were significant differences between high- and low-dose groups ($p < 0.05$ at all frequencies) (Figure S3A). In contrast, hearing recovery was not observed in *Otof*$^{-/-}$ mice receiving AAV1-hOTOF NT or AAV1-hOTOF CT alone (N- or C-terminal of human otoferlin) (Figure S4A). In addition, we analyzed the ABR wave I amplitude and latency of injected ears in the high-dose group at 1 month after injection. Although the amplitude, which represents the electrical responses of primary auditory neurons to the sound stimuli, was lower than the wild type (WT) (click stimulus at 90 dB; WT, 5.42 ± 0.68 μV; injected ears, 0.55 ± 0.10 μV; $p < 0.0001$) (Figure S5A), the latency was similar to WT (at 90 dB; WT, 1.43 ± 0.08 ms; injected ears, 1.59 ± 0.05 ms; $p = 0.08$) (Figure S5B). Furthermore, we also detected otoferlin expression in the high-dose group at 1 month after injection. Otoferlin was detected throughout the whole cochlear turns at a rate of 62.29% ± 3.80%, 69.62% ± 1.70%, and 76.56% ± 3.03% of the IHCs at the apical, middle, and basal turns, respectively (Figures 1F and 1G), whereas no otoferlin was detected in the cochlea injected with AAV1-hOTOF NT (Figure S4B).

The human inner ear is fully developed in the uterus in contrast to the mouse inner ear, which becomes fully mature at ∼3 weeks postnatally. To evaluate the relevance of our gene therapy approach for humans, we also injected AAV1-hOTOF into adult *Otof*$^{-/-}$ mice at P30 with different doses via the RWM and then tested their auditory function. At 2 weeks after injection, the click ABR thresholds in the injected ear of the adult *Otof*$^{-/-}$ mice were significantly rescued in the high-dose group (62.73 ± 2.73 dB), the intermediate- to high-dose group (63.06 ± 2.40 dB), and the intermediate-dose group (70 ± 2.77 dB), respectively (Figure 1C), which was consistent with the hearing improvement in neonatal *Otof*$^{-/-}$ mice. To assess the duration of hearing recovery, we measured the ABR thresholds in the injected ears of adult *Otof*$^{-/-}$ mice at 3 months after injection. Compared to the click ABR thresholds at 2 weeks after injection, hearing recovery remained stable in the high-dose group (61.36 ± 4.91 dB) and the intermediate- to high-dose group (65.88 ± 2.40 dB), with the best performer recovering to ∼40 dB, which was similar to WT mice. In contrast, in the intermediate-dose group, the click ABR thresholds were only moderately increased (75.83 ± 3.07 dB) (Figure 1D). To observe the long-term effects of hearing recovery, we also measured the click ABR thresholds in the injected ears of adult *Otof*$^{-/-}$ mice at 6 months after injection. Hearing recovery was still observed in the high-dose group (65.71 ± 3.35 dB) and the intermediate- to

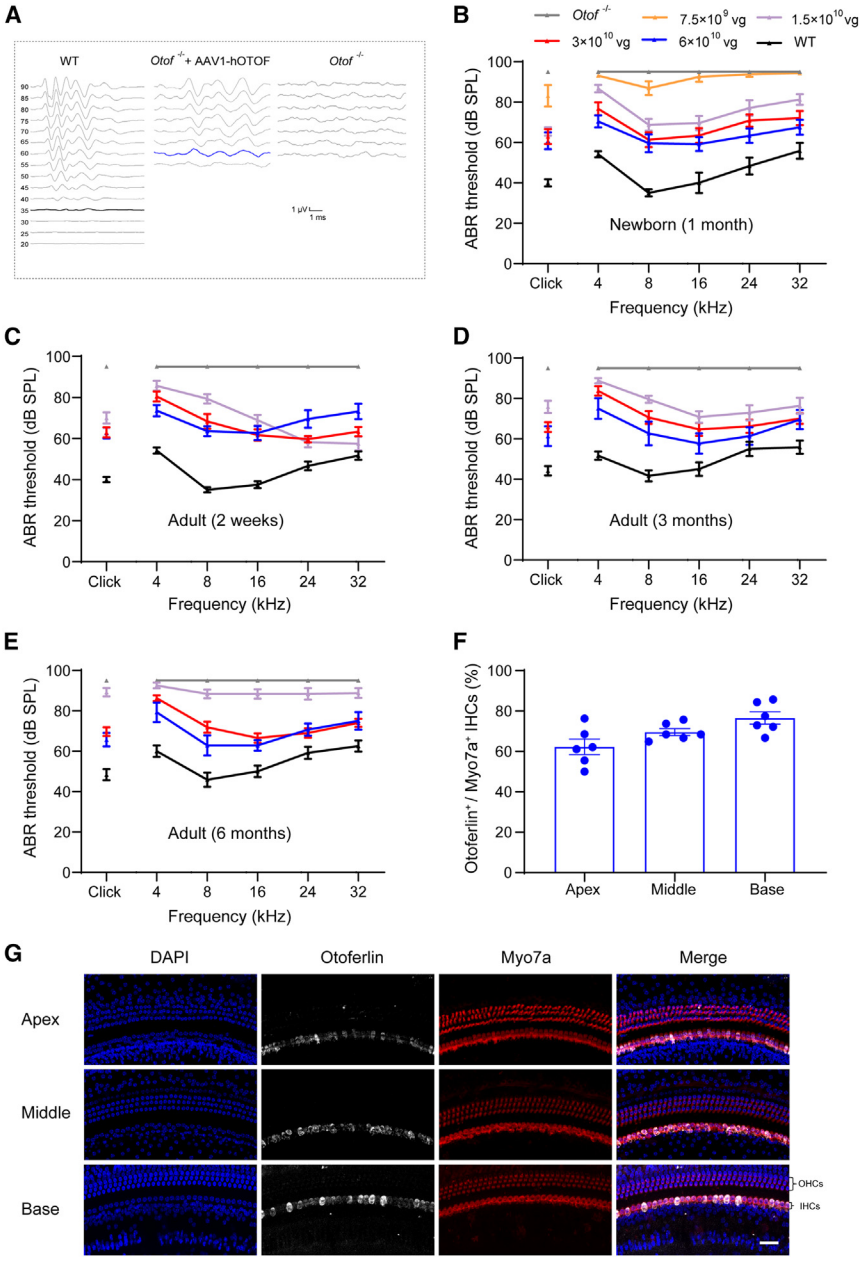

Figure 1. AAV1-hOTOF rescued hearing in *Otof*$^{-/-}$ mice

(A) Representative ABR traces in response to broadband click sound stimuli were recorded 4 weeks after therapy injection (6×10^{10} vg/cochlea) at P0–P2. (B) The ABR thresholds in the injected ear of *Otof*$^{-/-}$ mice were recorded 1 month after injection at P0–P2. (*Otof*$^{-/-}$, n = 8; WT, n = 6; 6×10^{10} vg/cochlea, n = 12; 3×10^{10} vg/cochlea, n = 12; 1.5×10^{10} vg/cochlea, n = 12; 7.5×10^{9} vg/cochlea, n = 8). (C) The ABR thresholds in the injected ear of adult *Otof*$^{-/-}$ mice were recorded 2 weeks after injection at P30 (*Otof*$^{-/-}$, n = 8; WT, n = 6; 6×10^{10} vg/cochlea, n = 11; 3×10^{10} vg/cochlea, n = 18; 1.5×10^{10} vg/cochlea, n = 14). (D) The ABR thresholds in the injected ear of adult *Otof*$^{-/-}$ mice were recorded 3 months after injection at P30 (*Otof*$^{-/-}$, n = 8; WT, n = 6; 6×10^{10} vg/cochlea, n = 11; 3×10^{10} vg/cochlea, n = 17; 1.5×10^{10} vg/cochlea, n = 12). (E) The ABR thresholds of adult *Otof*$^{-/-}$ mice were recorded 6 months after injection at P30 (*Otof*$^{-/-}$, n = 8; WT, n = 6; 6×10^{10} vg/cochlea, n = 7; 3×10^{10} vg/cochlea, n = 16; 1.5×10^{10} vg/cochlea, n = 12). (F and G) Otoferlin expression in the newborn *Otof*$^{-/-}$ mice injected with 6×10^{10} vg/cochlea observed at 1 month. The percentage of otoferlin-labeled IHCs in the injected ear (n = 6) (F). Representative images of IHCs immunostained with otoferlin, including the apical, middle, and basal turns (G). Scale bars: 20 μm. Data (B–F) are displayed as the mean ± SEM.

high-dose group (69.69 ± 2.16 dB). However, the click ABR thresholds were 89.17 ± 2.12 dB in the intermediate-dose group (Figure 1E). There were significant differences between high- and intermediate-dose groups at 4, 8, and 32 kHz at 2 weeks; at click and 8 kHz at 3 months; and at all frequencies at 6 months. However, the ABR threshold in the high-dose group was no different compared with the intermediate- to high-dose group at all frequencies at all time points (Figures S3B–S3D). These results support the fact that AAV1-hOTOF RWM delivery partially rescues hearing in adult *Otof*$^{-/-}$ mice long term with an efficacy that is positively correlated with an increasing dosage.

Auditory function was not affected in WT mice after AAV1-hOTOF injection

To evaluate whether the injection of AAV1-hOTOF via the RWM has adverse effects on the inner ear and hearing, we examined the auditory function and counted the number of HCs in WT mice. Adult WT mice were randomly assigned to the AAV1-hOTOF-injected or vehicle-injected groups. Limited by the space volume of the cochlea, the maximum dose of AAV1-hOTOF (6×10^{10} vg/cochlea, 2 μL) and an equal volume of vehicle were injected into adult WT mice. The ABR was assessed 2 weeks after injection. Compared with the contralateral uninjected ears, the ABR thresholds showed no changes in the injected ears across all frequencies in the two groups (Figures 2A and 2B). Furthermore, we performed immunohistochemistry and counted the number of HCs to observe the survival of HCs. There was no statistical difference between the injected ears and the contralateral uninjected ears, suggesting that AAV1-hOTOF did not cause obvious adverse effects and was well tolerated in the cochlea (Figures 2C–2F).

Biodistribution of AAV1-hOTOF in WT mice after RWM injection

Although local injection of AAV1-hOTOF into the inner ear provided an effective treatment for DFNB9 mouse models, few studies have comprehensively reported on the systemic biodistribution of

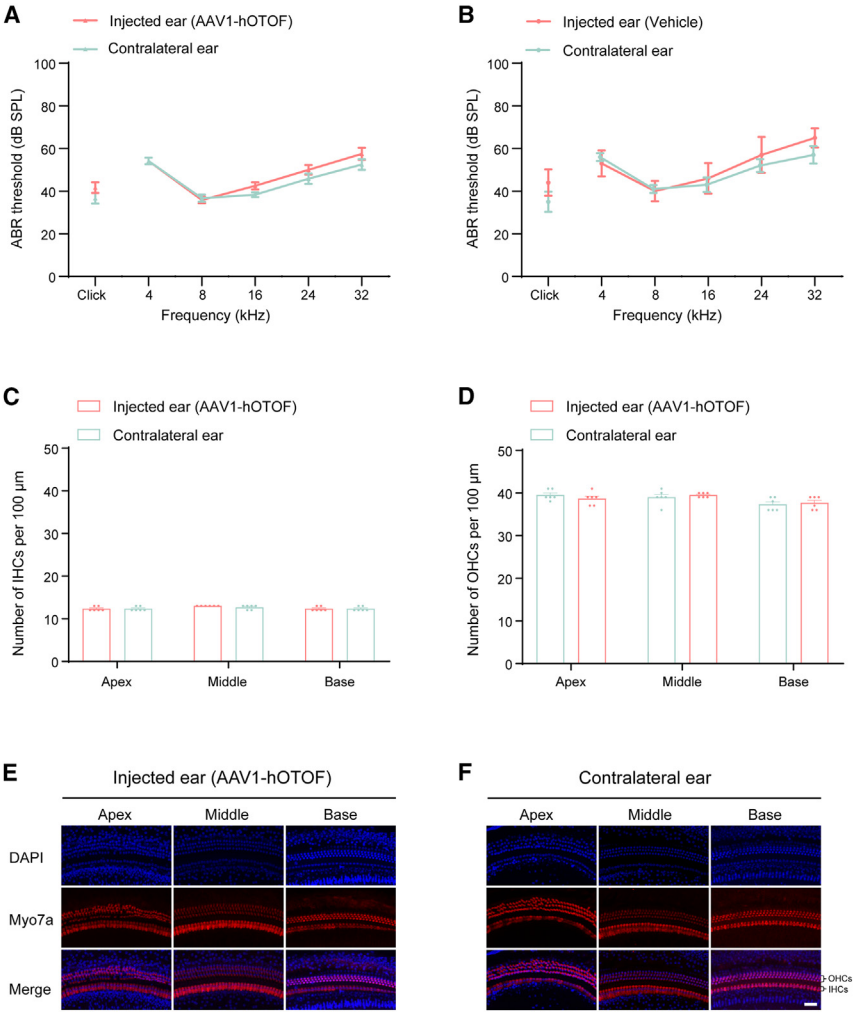

Figure 2. Auditory function was not affected in WT mice after AAV1-hOTOF injection

(A) The ABR thresholds of AAV1-hOTOF-injected (6×10^{10} vg/cochlea, 2 μL) and contralateral uninjected ears were recorded 2 weeks after injection (n = 6). (B) The ABR thresholds of vehicle-injected (2 μL) and contralateral uninjected ears were recorded 2 weeks after injection (n = 5). (C and D) These were quantified for IHCs (C) and OHCs (D). (E and F) Representative images of Myo7a-labeled HCs from the AAV1-hOTOF-injected (E) and contralateral uninjected ears (F) were observed at 2 weeks after injection. Scale bar, 20 μm. Data (A–D) are displayed as the mean ± SEM.

AAV1 in mice following local administration via the RWM. It is necessary therefore to assess the systemic biodistribution of AAV1-hOTOF related to its development in clinical application for gene therapy. To study the biodistribution of AAV1-hOTOF, the total DNA was extracted and analyzed by qPCR targeting AAV1-hOTOF NT to determine the viral genome copy number in the cochlea, brain, and liver, as well as other major organs at 6 weeks after injection. As expected, the injected ear had the highest copy number of vector genomes (1.2×10^6 vg/μg DNA) (Figure S6). The viral genome was 10^4–10^6 vg/μg DNA in the contralateral uninjected ear, brain, and spinal cord and at 10^3–10^4 vg/μg DNA in the liver, heart, spleen, and blood, whereas in other tissues the vector genome copy number was $<10^3$ vg/μg DNA (Figure S6). In summary, RWM injection yielded a high vector copy number in the cochlea, which was consistent with the treatment efficacy. The detection of a relatively high copy number of viral particles in the CNS and the liver suggests the necessity for careful safety assessment of potential toxicity in future clinical studies.

Normal behavior was not affected in WT mice after AAV1-hOTOF injection

To assess whether injected AAV1-hOTOF affects the general condition and behavior of mice, 2 μL of AAV1-hOTOF or vehicle was injected into adult WT mice cochlea, and behavioral tests, including the rotarod test, balance beam test, open field test, Y-maze test, and Irwin test were performed.

In the rotarod test, there was no significant difference in the falling time or falling speed between AAV1-hOTOF-injected and vehicle-injected groups ($p > 0.05$ for 2 and 4 weeks) (Figures 3A and 3B). In the balance beam test, all of the experimental animals succeeded in traversing the balance beam without falling off. The speed of the animals crossing the beam (both 1 cm and 2 cm wide) showed no statistical differences between the AAV1-hOTOF-injected and vehicle-injected groups ($p > 0.05$ for 2 and 4 weeks) (Figures 3C and 3D). In the open field test, we measured the distance traveled and time spent in the center region at 4 weeks after injection to quantify their locomotor activity and anxiety-like behaviors. The AAV1-hOTOF-injected mice traveled a distance in 30 min similar to that of the vehicle-injected group (90.20 ± 6.58 m versus 98.30 ± 7.87 m, $p = 0.44$) (Figure 3E). The time that AAV1-hOTOF-injected mice spent in the center region (61.62 ± 8.68 s) was comparable to that in the vehicle-injected group (79.65 ± 6.73 s) at 4 weeks after injection ($p = 0.12$) (Figure 3F). In the Y-maze test, the number of alterations, number of arm entries, and alteration percentage in the AAV1-hOTOF-injected group were similar to the vehicle-injected group at 4 weeks after injection ($p > 0.05$ for all comparisons) (Figures 3G–3I). The Irwin test was performed in mice at 1, 2, 3, and 4 weeks after injection. Between the two groups, no significant behavioral changes were observed in terms of general behaviors, convulsive behaviors and excitability, or reflex capabilities across the duration of the experiment (Table S1). No significant changes in the anus temperature were found between the two groups after injection (Figure S7). Overall, all of the experimental mice were healthy, and no

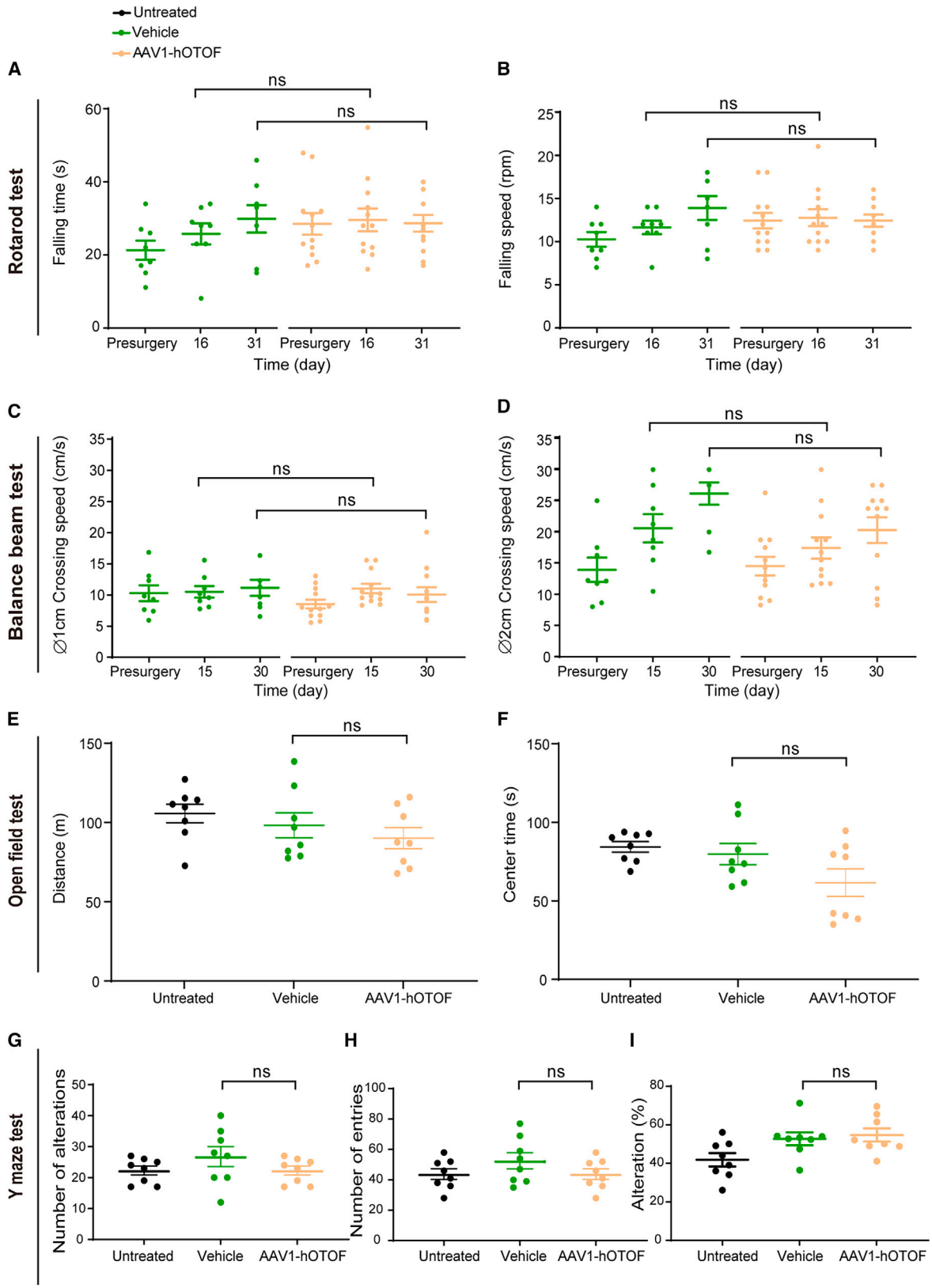

(legend on next page)

obvious behavioral changes could be attributed to the local injection of AAV1-hOTOF.

Abnormal clinical pathology was not observed in WT mice after AAV1-hOTOF injection

To further evaluate the potential systemic toxicity and inflammatory response to AAV1-hOTOF, mice from the AAV1-hOTOF-injected and vehicle-injected groups were phlebotomized at 6 weeks after injection, and the blood was analyzed by routine blood test and serum chemistry. For all of the routine blood test parameters, there were no statistical differences ($p > 0.05$ for all comparisons) between the AAV1-hOTOF-injected group and the vehicle-injected group (Table S2). No evidence of toxicity in serum chemistry was observed, and the values of hepatic function were comparable between the two groups ($p > 0.05$ for all comparisons) (Table S3). To evaluate the possible damage in the AAV1-hOTOF-injected and vehicle-injected mice 13 weeks after injection, histologic analysis was performed via H&E staining in the important organs, including the lung, liver, pancreas, colon, jejunum, kidney, brain, lymph nodes, spleen, bone marrow, skeletal muscle (thigh), and heart. Two vehicle-injected mice showed mild kidney inflammation, and one AAV1-hOTOF-injected mouse showed mild signs of inflammation in the colon. No pathological changes or signs of inflammation or fibrosis were observed in the remaining mice. We conclude that AAV1-hOTOF injection did not cause pathological inflammation (Figure S8).

Delivery of AAV1-GFP via RWM in the NHP inner ear results in efficient expression in HCs

Vector characterization in the NHP model is an important step before clinical trials. We investigated the expression of AAV1-delivered transgenes under the control of the HC-specific promoter *Myo15* in the inner ear of NHPs. Two *M. fascicularis* were injected (Table S4). The first one (animal 1) received AAV1-GFP (2.5×10^{11} vg in 20 μL vehicle) in the left ear via RWM injection using the trans-mastoid approach reported by Andres-Mateos et al.[42] For the second monkey (animal 2), we injected the left ear with a lower dose (1.5×10^{11} vg in 20 μL vehicle). Four weeks later, the animals were sacrificed and the temporal bone was extracted and decalcified over 2 months.

To evaluate the GFP expression in HCs, 40× images of each mapped frequency region were taken with a confocal microscope (Figures 4A, S9A, and S9B). Significantly, we detected GFP in the HCs but not in other regions of the cochlea. GFP^+ HCs were counted, and the values were plotted as a percentage of the total number of HCs. In the cochlea with high-dose injection, GFP^+ cells were detected in IHCs (apex, 63.16%; middle, 82.35%; base, 93.75%) and outer hair cells (OHCs) (apex, 37.82%; middle, 49.58%; base, 27.78%) (Figures 4B and 4C). In the cochlea with low-dose injection, GFP^+ cells were also detected in IHCs (apex, 65.38%; middle, 61.54%; base, 87.5%) and OHCs (apex, 37.74%; middle, 61.54%; base 24.24%) (Figures 4B and 4C). In addition, no GFP^+ cells were observed in the contralateral uninjected ear (Figure S9B). These results indicate that the AAV1 vector driven by the HC-specific *Myo15* promoter could mediate efficient and specific gene expression in HCs of the inner ear of NHPs.

Acute vector tolerability and biodistribution of AAV1-GFP in NHPs

We further evaluated systemic toxicity in NHPs after injection. NHPs were phlebotomized postsurgery (days 14 and 28), and blood was analyzed for routine blood test (Table S5) and serum chemistry (Table S6). Systemic toxicity was not detected by serum chemistry or routine blood test in injected NHPs, with the values mostly within the normal reference range based on a previous study,[43] although several parameters, such as albumin, aspartate aminotransferase, total bilirubin, and total protein, demonstrated some amount of fluctuation.

To study the biodistribution of AAV1-GFP in the injected NPHs, we assessed the viral genome copy number in the blood, brain, liver, and other peripheral tissues at 4 weeks after injection. Compared to other tissues, higher amounts of AAV1 were detected in the brain, spinal cord, and liver of NHPs with a high-dose injection (Figure 4D), whereas AAV1 was minimally detected in the liver of NHPs with a low-dose injection (Figure 4E). Overall, AAV1-GFP was well tolerated, and we did not observe any apparent systemic acute toxicity related to AAV1-GFP injections.

DISCUSSION

AAV-mediated gene therapy in humans has been applied successfully to treat genetic diseases, including hemophilia, neurological disorders, and blindness.[44–49] However, gene therapy for hereditary hearing loss has not reached a clinical stage. Here, in an effort to advance *OTOF* gene therapy to the clinical stage, we assessed the efficacy and safety of our AAV1-hOTOF agent in animal models. Our data showed that AAV1-hOTOF significantly rescued hearing in *Otof* $^{-/-}$ mice with profound hearing loss without obvious adverse effects. The hearing rescue was at least 6 months and seemed to positively correlate with an increasing dosage. Our results further demonstrated that the AAV1-transgene driven by the *Myo15* promoter was highly expressed in the HCs of the inner ear of NHPs and did not cause apparent systemic acute toxicity.

Figure 3. Normal behavior was not affected in WT mice after AAV1-hOTOF injection

(A and B) The rotarod performance of AAV1-hOTOF and vehicle-injected mice in falling time (A) and falling speed (B). (C and D) The speed of crossing the 1-cm (C) and 2-cm (D) balance beam were recorded from AAV1-hOTOF and vehicle-injected mice (A–D, AAV1-hOTOF group, n = 12; vehicle group, n = 8). (E and F) The open field performance of AAV1-hOTOF and vehicle-injected mice in the total traveled distances (E) and the time spent in the center region (F). (G–I) The Y-maze performance of AAV1-hOTOF and vehicle-injected mice in the number of alterations (G), number of entries (H), and the percentage of alteration (I) (E–I), untreated mice group, n = 8; AAV1-hOTOF group, n = 8; vehicle group, n = 8). Data (A–I) are displayed as the mean ± SEM. In (A–I), ns, not significant; *$p < 0.05$; **$p < 0.01$; ***$p < 0.001$; ****$p < 0.0001$; unpaired t test.

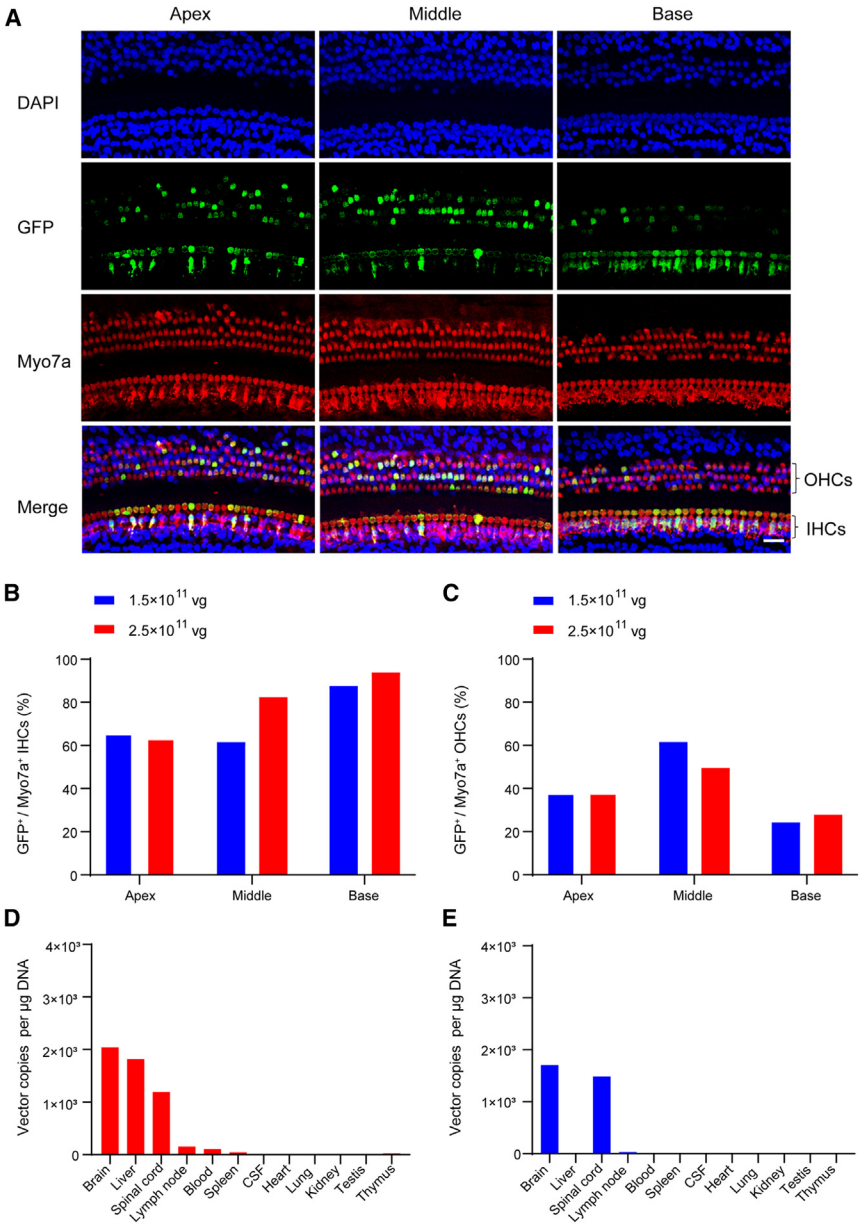

Figure 4. High expression of AAV1-GFP in NHP inner ear hair cells and the vector biodistribution via the RWM route

(A) Representative images of Myo7a-labeled HCs in the injected ear of NHPs at 4 weeks after injection with 2.5×10^{11} vg AAV1-GFP. Scale bar, 20 μm. (B and C) Expression efficiency of GFP in IHCs and OHCs from apex to base in the NHP cochlea injected with 2.5×10^{11} vg and 1.5×10^{11} vg. (D and E) Analysis of AAV1-GFP biodistribution in different organs from NHPs injected with 2.5×10^{11} vg (D) and 1.5×10^{11} vg (E). Samples were harvested 4 weeks after the injection (n = 2).

Previous studies have shown that gene replacement is a feasible strategy for gene therapy in *Otof*$^{-/-}$ mouse models,[15–17] and this was supported by our data. However, from a safety perspective, the design of our candidate drug was different from previous reports regarding the key constituent elements important in the clinic, especially the AAV delivery vector and promoter. Because there are no cell-specific AAVs for the cochlea currently, AAV1 is commonly applied in clinical trials with good safety records,[29–33] and HC-specific promoters will be the ideal choice for constructing gene therapy drugs for the treatment of DFNB9. For this reason, we selected AAV1 with the tropism primarily in IHCs as a delivery tool and designed a candidate drug (AAV1-hOTOF) driven by the *Myo15* promoter[34–36] to further confine the expression of hOTOF to HCs. We hypothesized that our approach could decrease the ectopic expression of hOTOF via local injection compared to the therapeutic systems used in previous reports.

To test this hypothesis, we injected AAV1-hOTOF into mouse models by the route of RWM. As expected, high expression of otoferlin specifically in HCs was detected, which may be very beneficial for human gene therapy applications by avoiding potential off-target effects. We found that AAV1 was predominately distributed in the inner ears, although AAV1 was also detected in the CNS and liver. One reason for the distribution of AAV1 in other organs may be the cochlear aqueduct, which is a communication channel between the cerebrospinal fluid (CSF) and the perilymph; another reason may be internal auditory meatus or modiolus, providing a probable pathway.[50–54] In our study, the high-dose injection did not affect the normal behavior, the hepatic function, and the normal function of other major organs in WT mice, which suggests a profile of safety and tolerability of AAV1-hOTOF for future use in clinical studies.

NHPs are phylogenetically close to humans in physiology, anatomy, immunology, and neurology, all of which make them excellent experimental models to assess the toxicity and pharmacology of vector systems before consideration for preclinical studies.[27,42,55,56] In our study, AAV1-GFP showed good efficiency in transducing the cochlear HCs in NHPs. Compared to the previous study,[42] we detected relatively higher GFP expression in HCs with no transduction of other cell types along the length of the cochlea following RWM injection in NHPs. There are several possible explanations for the expression discrepancy between our study and the previous study. First, this could be due to preexisting immunity to AAV in the perilymph that affects the transduction of the cochlea, because the significant correlation between the titers of antibody and the levels of GFP expression has been shown

previously.[57] It may be necessary to detect neutralizing antibodies against AAV before injecting the AAV-mediated gene therapy system. Second, the small anatomical size and limited exposure of the oval and round window may result in differences in AAV delivery during the surgical procedure. Third, other factors that may explain the discrepancies include the promoter, vector quality, volume, duration of study, the age of the animal at the time of surgery, and the animal species.[58]

Biodistribution in the CNS and systemic biodistribution were also quantified in our study. In a previous study, a patent cochlear aqueduct together with local AAV injection resulted in the transduction of cerebellar Purkinje cells in mice.[51] Although there is still debate about the patency of the cochlear aqueduct in NHPs and humans,[59,60] the majority of adult human temporal bones are more likely to be occluded with loose connective tissue.[61] However, some investigators believe that the cochlear aqueducts are patent in humans, which does not preclude the possibility of the viral vectors reaching the CNS after inner ear injection.[62,63] In our study, no GFP expression was detected in the contralateral uninjected ear, and AAV1 genome copies were detected at a low level in the CNS tissue, followed by the spinal cord and the liver, whereas other peripheral tissues had relatively lower vector copies in NHPs. There was no evidence of toxicity observed by serum chemistry and routine blood tests, although a few differences were detected in some parameters, suggesting the safety of the AAV1 vector carrying the *Myo15* promoter and the *GFP* or *OTOF* transgene, which may further strengthen the safety profile. We will continue to expand the number of NHPs with longer follow-up in future studies.

The human cochlea is fully developed *in utero*, whereas the rodent cochlea is not mature until 3 weeks after birth.[64] The cochlea is a relatively isolated organ compared to systemic injection, and local injection in the inner ear tends to result in a high drug concentration inside the cochlea and to minimize the distribution in other organs. Therefore, successful gene therapy in the mature inner ear is more relevant for translational application in the clinic. The RWM route, delivering therapeutic agents into the scala tympani, is one of the most common approaches for gene therapy in adult mice,[65–67] but a novel delivery strategy that combines RWM injection with canalostomy has demonstrated highly efficient transduction throughout the cochlea and minimal hearing impairment in rodents.[65,66] In previous studies, the invasive trans-mastoid approach of RWM injection after making a fenestra in the oval window was implemented successfully in NHPs.[42,68] The human cochlea has more space to operate than does the NHP cochlea. We thus expect the approach of RWM injection with canalostomy or making a fenestra in the oval window to be a feasible gene transfer method for gene therapy to treat deafness in humans.

In summary, our study established a therapeutic agent, AAV1-hOTOF, for DFNB9 and demonstrated its efficacy and safety in mouse models. In addition, we explored the transduction and tolerance of AAV1-GFP in NHPs. These findings strongly support the clinical development of AAV1-hOTOF.

MATERIALS AND METHODS

Mice

Details of the *Otof* $^{-/-}$ mice, established by BIOCYTOGEN (Beijing, China), are described in our previous study.[15] WT mice (129 strain) were used in the experiments to evaluate the AAV1-hOTOF. All of the mice were raised in the Department of Laboratory Animal Science of Fudan University, with free access to food and water and 12-h light/dark cycles. All of the animal experiments were performed according to guidelines regarding institutional animal welfare and were approved by the Animal Care and Use Committee of Fudan University, China.

Construction of dual-AAV strategies

For the therapeutic agent constructs, the full-length human *OTOF* CDS (NM_001287489.2) was split at the exon 21-exon 22 junction site, which was divided into 5′ terminal and 3′ terminal segments referring to the previous study.[17] The human *OTOF* CDS was synthesized by Sangon Biotech (Shanghai, China). The 5′ terminal and 3′ terminal segments were packaged into the AAV1 capsid. Both otoferlin dual-5′ AAV1-TS and 5′ AAV1-Hyb half-vectors carried the CAG or *Myo15* promoter (patent no.: US 2021/0388045 A1), the 5′ terminal segment of the *OTOF* CDS, and an SD sequence.[39] The dual-3′ AAV1-TS and 3′ AAV1-Hyb half-vectors carried an SA sequence, the 3′ terminal segment of the *OTOF* CDS, a woodchuck hepatitis virus posttranscriptional regulatory element (WPRE), and a bovine growth hormone polyadenylation sequence (pA). In addition, the highly recombinogenic sequence derived from the AK or AP was added downstream of the SD sequence and upstream of the SA sequence in the dual-5′ AAV1-Hyb and 3′ AAV1-Hyb half-vectors.[39] The therapeutic system of the dual-AAV1-Hyb (AK) approach in which the human *OTOF* CDS was driven by *Myo15* promoter was abbreviated as AAV1-hOTOF. The N- and C-terminal of human *OTOF* packaged by AAV1 were called AAV1-hOTOF NT and AAV1-hOTOF CT, respectively.

Virus production

The AAV2 inverted terminal repeats were used as a packaging signal for packaging with the AAV1 serotype. The AAVs used in this study include AAV1-CAG-hOTOF NT-AK, AAV1-CAG-hOTOF NT-AP, AAV1-CAG-hOTOF NT-TS, AAV1-*Myo15*-hOTOF NT-AK, AAV1-*Myo15*-hOTOF NT-AP, AAV1-*Myo15*-hOTOF NT-TS, AAV1-hOTOF CT-AK, AAV1-hOTOF CT-AP, AAV1-hOTOF CT-TS, and AAV1-*Myo15*-GFP-WPRE-bGH-polyA. The vector plasmid together with capsid and helper plasmids were transiently transfected into HEK293T cells to produce viral particles. The viruses were commissioned from PackGene Biotech (Guangzhou, China). After determination of the virus genome titers by qPCR and each titer was adjusted to 3×10^{13} vg/mL, all of the viruses were stored at −80°C. Before injection, viral titers of dual vectors (5′ and 3′ terminals) were thawed and mixed in a 1:1 ratio.

Expression and recombination of otoferlin in HEK293T cells

The HEK293T cells were cultured in high-glucose DMEM with 10% fetal bovine serum and penicillin/streptomycin (catalog no.

11965092, Thermo Fisher Scientific, Waltham, MA) in a humidified incubator free from mycoplasma and chlamydia at 5% CO_2 and 37°C. Based on three different recombination strategies, AAV1-CAG-hOTOF NT and AAV1-hOTOF CT were used to infect HEK293T cells by MOI 2×10^5. After 48 h, the cells were lysed in cold radioimmunoprecipitation assay buffer (catalog no. P0013B, Beyotime, Jiangsu, China) containing PMSF (catalog no. ST506, Beyotime) to release otoferlin, and the total protein concentration was determined using a bicinchoninic acid protein assay kit (catalog no. P0012S, Beyotime). The protein samples were separated by SDS-PAGE (4%–12% Bis-Tris gels, catalog no. M41210C, Genscript, Piscataway, NJ) with 3-(*N*-morpholino)propanesulfonic acid (MOPS) buffer (Tris-MOPS-SDS Running Buffer, catalog no. M00138, Genscript) and were transferred onto polyvinylidene fluoride membranes. The membranes were probed with the primary antibodies rabbit immunoglobulin G (IgG) anti-OTOF (1:2,000 dilution, catalog no. PA5-52935, Thermo Fisher Scientific), rabbit IgG anti-glyceraldehyde 3-phosphate dehydrogenase (1:1,000 dilution, catalog no. 5188, Cell Signaling Technology, Danvers, MA), and followed by incubation with the anti-rabbit IgG-horseradish peroxidase secondary antibody (1:2,000 dilution, catalog no. A0239, Beyotime). Finally, the secondary antibodies were detected using Western Blot ECL Blotting Substrate (catalog no. 34580, Thermo Fisher Scientific) with a Tanon 4600 system.

Inner ear injection

The surgical procedure of inner ear injection via the RWM was as described previously.[15,69] Briefly, P0–P2 mice were anesthetized by hypothermia on ice. Cochleostomy was performed by postauricular incision to expose the cochlear bulla, and a glass micropipette (WPI, Sarasota, FL) connected to a nanoliter microinjection system (WPI) was used to manually deliver the AAV1-hOTOF into the inner ear via RWM. The operation was conducted only in the right ear of each animal. The incision was closed with sutures after the injection, and the mice were placed on a heating pad (37°C) for resuscitation and then returned to their cage.

Adult mice were anesthetized with ketamine (100 mg/kg) and xylazine (10 mg/kg) via intraperitoneal injection. The operated postauricular region was exposed by shaving and was disinfected with 10% povidone-iodine. Surgery was performed under an operating microscope. We made a 10-mm postauricular incision to access the temporal bone and subsequently drilled a small hole in the tympanic bulla to expose the round window. A glass micropipette held by a nanoliter microinjection system was used to penetrate the RWM and it was left open for a few minutes until no obvious perilymph leakage was observed. We performed the vector or vehicle (PBS with 0.001% PF68) delivery with an injection rate of 5 nL/s controlled by the Nanoliter Microinjection Controller (WPI). The RWM niche was sealed with a small plug of muscle quickly after the injection, and then the otic bulla was sealed with muscle using tissue adhesive. The skin was closed with sutures.

Hearing test

The ABR was recorded in a soundproof chamber using the TDT BioSigRP system (Tucker-Davis Technologies, Alachua, FL) as previously described.[14,15,70] Mice of either sex were anesthetized through intraperitoneal injection with xylazine (10 mg/kg) and ketamine (100 mg/kg).[15,70] The recording electrode, the reference electrode, and the ground electrode were inserted at the mastoid portion, the subcutaneous tissues of the vertex, and the rump of the mice, respectively. We examined the mice to exclude otitis media or the abnormal formation of cerumen in the ear canal before recording. The sound level was decreased in 5-dB steps from 90 dB to 20 dB SPL. Tone burst acoustic stimuli were presented at 4, 8, 16, 24, and 32 kHz. The ABR responses were amplified (10,000×), filtered (0.3–3 kHz), and averaged (1,024 responses) at each SPL. The ABR threshold was defined as the lowest SPL level at which any wave could be visually detected and repeated. In addition, the amplitude of wave I of the ABR was measured by the difference between the peak of wave I and the following trough. The acoustic stimuli thresholds were defined by two independent observers.

Behavioral test

Rotarod test

A mouse rotary rod instrument was used to assess the ability of motor coordination and motor learning of the mice.[71] In the training session, the mice were placed on a rotating rod with a diameter of 3 cm to acclimate to the equipment, and the speed was set to 8 rpm. In the test session, mice were placed on a slowly moving rod and the rotation speed was accelerated from 4 to 40 rpm in 5 min. The time and the rotation speed when the mouse fell off were recorded. The apparatus was cleaned to prevent the residual information from the previous mouse from affecting the test results.

Balance beam test

The balance beam test was used to assess the motor coordination and balance of mice.[71] The beam (1 or 2 cm wide, 100 cm length) was elevated 50 cm. A black plastic box ($30 \times 15 \times 15$ cm) was set as a nest at the end of the beam for motivating the animal to cross the beam. Cloth was placed under the equipment to protect the animals from injury if they fell off. The balance beam was cleaned with 75% alcohol and then water between trials. Before the test, the mouse was allowed to rest in the box for 3 min, then placed on the beam 60 cm from the endpoint. After the test, the time and the average movement speed of mice to cross the beam were recorded. If the animal fell off, the distance and time that the animal actually crawled on the beam were recorded, then the mouse was placed in the box to rest for 1 min, and the previous steps were repeated three times.

Open field test

The open field test was used to assess locomotor activity and anxiety-related behaviors of the mice.[72,73] During the test, each mouse was placed in the center of a plastic chamber ($50 \times 50 \times 40$ cm), and the movement was recorded for 30 min with a video tracking system. After the test, the mouse traveled distance and the time in the center

region were analyzed. The chamber was cleaned with 75% alcohol and then water to avoid olfactory cues.

Y-maze test

The Y-maze consisted of three equiangular arms that were labeled A, B, and C and was used to evaluate the spatial memory of mice.[74] Mice were placed in the center of the maze and allowed to visit three arms freely for 8 min. The number of arm entries and alternations were recorded. The alteration was determined from successive consecutive entries to the three different arms, such as ABC, BCA, and BAC. The alteration was expressed as the percentage of alternations and was calculated as (alternations/[total arm entries – 2]) × 100.

Irwin test

The Irwin test was developed to detect any deleterious effects of a new drug on general behavior. Each mouse was observed in a transparent box, and the observation consisted of the general behavior (spontaneous exploration, grooming, smelling its congeners, normal resting state, alertness, distending/edema, bad condition, moribund, and dead), convulsive behavior and excitability (spontaneous activity, restlessness, fighting, writhing, tremor, stereotypy, twitches/jerks, Straub, opisthotonos, and convulsion), and reflex capabilities (startle response, touch reactivity, vocalization, abnormal gait, corneal reflex, pinna reflex, catalepsy, grip reflex, pulling reflex, righting reflex, body tone, and pain response). The incidence rate and severity of the symptoms were analyzed. The rectal temperature of each mouse was measured after observation. The behavioral tests, including the rotarod test, balance beam test, open field test, Y-maze test, and Irwin test, were performed by WuXi AppTec (Shanghai, China) and PharmaLegacy Laboratories (Shanghai, China).

Immunohistochemistry

Cochleae were harvested immediately after the mice were sacrificed and they were fixed in 4% paraformaldehyde (PFA; catalog no. E672002-0500, Sangon Biotech, Shanghai, China) at 4°C overnight. A small hole was then made at the apex of the cochlea to facilitate PFA irrigation, and the cochleae were decalcified in 10% EDTA; catalog no. E671001-0500, Sangon Biotech) for 2–3 days. The basilar membrane from the decalcified cochlea was dissected and cut into pieces for immunofluorescence. These membranes were infiltrated with 1% Triton X-100 (catalog no. A110694, Sangon Biotech) in PBS, and blocked in 5% donkey serum (catalog no. D9663, Sigma-Aldrich, St. Louis, MO) for 1 h at room temperature. After that, the tissues were incubated with mouse IgG1 anti-otoferlin (1:200 dilution, catalog no. ab53233, Abcam, Cambridge, UK) and the rabbit anti-Myo7a (1:500 dilution, catalog no. 25–6790, Proteus BioSciences, Waltham, MA) primary antibodies overnight at 4°C, followed by three washings with PBS. The appropriate Alexa Fluor 555-conjugated anti-mouse IgG1 (1:500 dilution, catalog no. A21127, Invitrogen, Carlsbad, CA) and Alexa Fluor 647-conjugated anti-rabbit (1:500 dilution, catalog no. A31573, Invitrogen) secondary antibodies were then incubated for 2 h at room temperature. The cell nuclei were stained with DAPI (catalog no. F6057, Sigma-Aldrich). Images were collected on a Leica TCS SP8 laser scanning confocal microscope with a 40× objective. The images were processed and analyzed with ImageJ software. For IHC and OHC counting, the numbers of $Myo7a^+$ HCs and the numbers of $GFP^+/Myo7a^+$ cells were counted in every nonoverlapping 100-μm region of the apical, middle, and basal turns of the basilar membrane.

Tissue biodistribution of vector DNA

Mice were anesthetized with 5% isoflurane and immediately sacrificed by decapitation. Different tissues and organs, including the lymph nodes, pancreas, spinal marrow, thymus, heart, liver, spleen, lung, kidney, testicle, and brain, were carefully dissected and separated. Viral DNA was extracted and purified from tissues using a QIAamp DNA Mini Kit (catalog no. 51304, Qiagen, Hilden, Germany) following the manufacturer's instructions and were dissolved in nuclease-free water. The DNA concentration was measured by spectrophotometric analysis using a NanoDrop spectrophotometer (Thermo Fisher Scientific). A sufficient volume was calculated such that 500 ng DNA was used for each PCR reaction. qRT-PCR was used to determine the copy number of AAV1-hOTOF NT in different tissues on a QuantStudio 1 Real-Time PCR instrument (catalog no. INS-0049, Thermo Fisher Scientific) using TaqMan probes and primers for the 5′ terminal (1–2,523 bp) segment of OTOF and AK region and the AceQ qPCR Probe Master Mix (catalog no. Q112-02, Vazyme, Beijing, China). The forward primer and reverse primer were used for these experiments (*Myo15*-Otof-AK-N forward: 5′-CTGAGGCTGTGCCAGAACT-3′; *Myo15*-Otof-AK-N reverse: 5′-GCAAAATCCCAGAAACGCAAGAG-3′; *Myo15*-SD-AK probe: 5′FAM-TCCTGGCGGACGAGGTAAGTATCAAGG-3′BHQ1). Each 20-μL reaction mixture contained 12.5 μL of AceQ qPCR Probe Master Mix, 0.5 μL of Rox dye (type II), 5.75 μL of RT-PCR grade H_2O, 0.5 μL (10 μM) each of forward and reverse primer, 0.25 μL (10 μM) of probe primer, and 5 μL (100 ng) of DNA sample. All of the samples were run in triplicate. Two nontemplate control reactions (20 μL) and one RNase/DNase-free H_2O blank (20 μL) were included in each run. The 96-well plates were sealed with an optically clear seal (Applied Biosystems, Waltham, MA), and the PCR cycling conditions included 5 min at 95°C, and then 40 cycles of denaturation for 15 s at 95°C and annealing and extension for 30 s at 60°C. The concentrations of PCR product were interpolated from the cycle threshold (CT) values, and triplicate concentration values were averaged.

Routine blood test and serum chemistry in mice

Mice were anesthetized with 5% isoflurane and immediately sacrificed. Blood samples (1.5–2.0 mL) were taken from mice, which were used for routine blood test and serum chemistry. Routine blood test and serum chemistry were performed by WuXi AppTec.

H&E staining

Samples from mice tissues and organs were fixed in 10% formalin buffer, embedded with paraffin, sectioned, stained with H&E, and evaluated by experienced veterinary anatomic pathologists. H&E staining was performed according to the standard protocols at PharmaLegacy Laboratories (Shanghai, China).

NHPs

M. fascicularis were kindly provided and accommodated by PharmaLegacy Laboratories (Shanghai, China). The NHP experiments were approved by the Institutional Animal Care and Use Committee of Fudan University and the Shanghai Medical Experimental Animal Administrative Committee. The subjects used for experimentation were 5- to 7-year-old males. Every animal was healthy and without ear disease or otologic surgery history, such as ear infections, signs of imbalance, or other risk factors for the loss of inner or middle ear function. A psychologically and physically comfortable environment was provided for the animals with a room temperature of 18°C–28°C, humidity of 30%–70%, and a 12-h light/dark cycle.

Venous blood and CSF sampling in NHPs

Blood was collected intravenously at 14 and 28 days postsurgery after sterilizing the epidermis of the femoral vein or saphenous vein with 75% alcohol in sedated animals. A standard vacutainer needle was inserted into the vein, and a swab was used to apply pressure to the vessel after the removal of the needle to achieve hemostasis. NHP serum chemistry and routine blood test in the monkeys were performed by Shanghai PharmaLegacy Laboratories (Shanghai, China).

CSF was obtained from the cisterna magna before the sacrifice of the monkeys. Atropine was given preoperatively. Once general anesthesia was established, we removed the hair from the epidermis of the cisterna magna and disinfected the skin with 75% alcohol. After that, the neck of the animal was bent to better expose the area. A 23G needle was used to collect the CSF sample.

RWM injection surgery in NHPs

The protocol was performed according to a previous study.[42] After the general anesthesia was established, the animal was intubated with a reinforced endotracheal tube. The surgical region was exposed by shaving and then disinfected with 10% povidone-iodine. A 25-mm semilunar incision was made, and the mastoid cortex was exposed. Bipolar electrocautery was used for meticulous hemostasis during the operation. Self-holding retractors was placed, and the surgical microscope was used. The external auditory canal wall, tympanic membrane, facial nerve, and chorda tympani were protected during the surgery. After the round window niche and the stapes footplate were visualized, a fenestration in the oval window was made with a needle and observed for a few minutes until no obvious perilymph leakage was found. The bony overhangs of the round window niche were gently removed to expose the RWM.

A nanoliter microinjection system (WPI) connected to an injection needle was used to deliver the AAV1-GFP at a rate of 1 μL/min for ?20 min. A total of 20 μL AAV1-GFP was microinjected into the scala tympani through the RWM. After the injection, the RWM and the fenestra in the stapes footplate were sealed with muscle. The mastoid cavity was blocked with bone meal and adjacent autologous tissue, and the skin was closed with sutures. During the postoperative care period, the animals were carefully monitored and in good care.

Immunohistochemistry and histology experiments of NHPs

The protocol was performed according to a previous study.[42] All of the animals were euthanized without recovery from the deep anesthesia. In brief, the carotid artery was exposed and adequately perfused with saline, followed by formalin solution to achieve full irrigation and preliminarily fixation of the inner ear sample. Cochlear samples and samples from different organs were harvested and processed for histological and/or biodistribution studies.

The cochlear samples were fixed in 4% PFA (catalog no. E672002-0500, Sangon Biotech) and decalcified in 10% EDTA (catalog no. E671001-0500, Sangon Biotech) at 4°C with regular trimming for ? 2 months. The basilar membrane collected from the cochlea was permeabilized with 1% Triton X-100 (catalog no. A110694, Sangon Biotech) in PBS and blocked in 5% donkey serum (catalog no. D9663, Sigma-Aldrich) for 1 h at room temperature. DAPI (catalog no. F6057, Sigma-Aldrich) was used to stain the cell nucleus. The primary antibodies were rabbit anti-Myo7a (1:500 dilution, catalog no. 25–6790, Proteus BioSciences) and chicken IgY anti-GFP (1:500 dilution, catalog no. ab13970, Abcam), and the following secondary antibodies were Alexa-conjugated donkey anti-rabbit IgG [H + L], Cy3 (1:500 dilution, catalog no. 711-165-152, Jackson ImmunoResearch, West Grove, PA), and Alexa Fluor 488-conjugated anti-chicken IgY (1:500 dilution, catalog no. A11039, Invitrogen). A Leica TCS SP8 laser scanning confocal microscope was used to collect the fluorescent z stack images (40× objective). The maximum intensity projections of the optical confocal sections are shown in the figures. The images were processed and analyzed using ImageJ software. For the quantification of GFP^+ cells, all of the images obtained with the 40× objective of every mapped frequency region (nonoverlapping) were manually quantified along the full length of the basilar membrane by two independent researchers who were blinded to the treatment. The percentages were obtained by dividing the number of GFP^+ cells by the total number of $Myo7a^+$ HCs (IHCs and OHCs were calculated separately).

Tissue DNA extraction and qPCR

Different organ tissues were harvested, weighed, and homogenized in buffered Proteinase K and incubated overnight at room temperature, followed by centrifuging for 10 min at 10,000 × *g* at 4°C to a final concentration of 100 μg/mL. Total DNA was extracted using a DNA mini-kit (catalog no. 51304, Qiagen) according to the manufacturer's instructions. qRT-PCR was carried out using the QuantStudio 1 Real-Time PCR Detection System (catalog no. INS-0049, Thermo Fisher Scientific). Forward primer: 5′-GCTATTGCTTCCCGTATGGC-3′; reverse primer: 5′-GGAAAGGAGCTGACAGGTGG-3′. Each PCR reaction contained 12.5 μL of SYBR Premix Ex TaqIIMix, 8.5 μL of ddH_2O, 1 μL (10 μM) each of the forward and reverse primers, and 2 μL of the DNA sample. All of the samples were run in triplicate. Two nontemplate control reactions (25 μL) and one RNase/DNase-free H_2O blank (25 μL) were included in each run. The 96-well plates were sealed with an optically clear seal (Applied Biosystems), and the reactions were carried out with an initial incubation at 95°C for 30 s, followed by 40 cycles of denaturation at 95°C for 5 s, annealing at

60°C for 30 s, and extension at 60°C for 30 s. All of the reactions were carried out in triplicate, and the nontemplate controls containing water instead of template DNA were included in every PCR run.

Statistical analyses

Data are depicted as the mean and SEM. Statistical analysis was performed and plotted using GraphPad Prism 9 (GraphPad, La Jolla, CA). An unpaired t test was used to test for statistical significance between two nonpaired normally distributed data groups. The statistical significance in parametric multiple comparisons was tested by Tukey's multiple comparison test following the one-way ANOVA test or the two-way ANOVA test. In addition, Dunn's multiple comparison test following the Kruskal-Wallis test was used to test for statistical significance in nonparametric multiple comparisons. Statistical significance is indicated in the figures: ns, not significant; *$p < 0.05$; **$p < 0.01$; ***$p < 0.001$; ****$p < 0.0001$.

DATA AND CODE AVAILABILITY

All of the study data generated in the article and/or supplemental information during the present study are available from the corresponding author on reasonable request.

SUPPLEMENTAL INFORMATION

Supplemental information can be found online at https://doi.org/10.1016/j.omtm.2023.101154.

ACKNOWLEDGMENTS

This work was supported by the National Natural Science Foundation of China (82225014, 82171148, and 82192864), the National Key R&D Program of China (2020YFA0908201 and 2021YFA1101302), the Shanghai Municipal Health Commission (20224Z0003), the Science and Technology Commission of Shanghai Municipality (21S11905100), the Shanghai Municipal Education Commission (2023ZKZD12), the Shuguang Program (20SG08) supported by the Shanghai Municipal Education Commission and the Shanghai Education Development Foundation, and Fudan University (yg2022-23). We also acknowledge the Ines-Fredrick Yeatts Inner Ear Research Fund (to Z.-Y.C.).

AUTHOR CONTRIBUTIONS

Y.S., H.L., and B.C. developed and supervised the project. L.Z., H.W., M.X., J.W., and J.L., performed the experiments. L.Z., H.W., M.X., and H.T. analyzed the data for the project and wrote the manuscript. Y.S., Z.-Y.C., L.Z., Y.C., D.W., Z.G., J.W., H.T., S.H., and B.Z. reviewed and revised the manuscript. All of the authors read and approved the final manuscript.

DECLARATION OF INTERESTS

The authors declare no competing interests.

REFERENCES

1. WHO (2021). Deafness and Hearing Loss. https://www.who.int/news-room/fact-sheets/detail/deafness-and-hearing-loss.
2. Lieu, J.E.C., Kenna, M., Anne, S., and Davidson, L. (2020). Hearing Loss in Children: A Review. JAMA *324*, 2195–2205.
3. Morton, C.C., and Nance, W.E. (2006). Newborn hearing screening–a silent revolution. N. Engl. J. Med. *354*, 2151–2164.
4. Nishio, S.Y., and Usami, S.I. (2017). Outcomes of cochlear implantation for the patients with specific genetic etiologies: a systematic literature review. Acta Otolaryngol. *137*, 730–742.
5. Rouillon, I., Marcolla, A., Roux, I., Marlin, S., Feldmann, D., Couderc, R., Jonard, L., Petit, C., Denoyelle, F., Garabédian, E.N., and Loundon, N. (2006). Results of cochlear implantation in two children with mutations in the OTOF gene. Int. J. Pediatr. Otorhinolaryngol. *70*, 689–696.
6. Chang, Q., Wang, J., Li, Q., Kim, Y., Zhou, B., Wang, Y., Li, H., and Lin, X. (2015). Virally mediated Kcnq1 gene replacement therapy in the immature scala media restores hearing in a mouse model of human Jervell and Lange-Nielsen deafness syndrome. EMBO Mol. Med. *7*, 1077–1086.
7. Wesarg, T., Richter, N., Hessel, H., Günther, S., Arndt, S., Aschendorff, A., Laszig, R., and Hassepass, F. (2015). Binaural integration of periodically alternating speech following cochlear implantation in subjects with profound sensorineural unilateral hearing loss. Audiol. Neurootol. *20*, 73–78.
8. Jiam, N.T., Caldwell, M.T., and Limb, C.J. (2017). What Does Music Sound Like for a Cochlear Implant User? Otol. Neurotol. *38*, e240–e247.
9. Stickney, G.S., Zeng, F.G., Litovsky, R., and Assmann, P. (2004). Cochlear implant speech recognition with speech maskers. J. Acoust. Soc. Am. *116*, 1081–1091.
10. Meister, H., Walger, M., Lang-Roth, R., and Müller, V. (2020). Voice fundamental frequency differences and speech recognition with noise and speech maskers in cochlear implant recipients. J. Acoust. Soc. Am. *147*, EL19.
11. Johnson, L.A., Della Santina, C.C., and Wang, X. (2016). Selective Neuronal Activation by Cochlear Implant Stimulation in Auditory Cortex of Awake Primate. J. Neurosci. *36*, 12468–12484.
12. Limb, C.J., and Roy, A.T. (2014). Technological, biological, and acoustical constraints to music perception in cochlear implant users. Hear. Res. *308*, 13–26.
13. Tao, Y., Liu, X., Yang, L., Chu, C., Tan, F., Yu, Z., Ke, J., Li, X., Zheng, X., Zhao, X., et al. (2022). AAV-ie-K558R mediated cochlear gene therapy and hair cell regeneration. Signal Transduct. Target. Ther. *7*, 109.
14. Xue, Y., Hu, X., Wang, D., Li, D., Li, Y., Wang, F., Huang, M., Gu, X., Xu, Z., Zhou, J., et al. (2022). Gene editing in a Myo6 semi-dominant mouse model rescues auditory function. Mol. Ther. *30*, 105–118.
15. Tang, H., Wang, H., Wang, S., Hu, S.W., Lv, J., Xun, M., Gao, K., Wang, F., Chen, Y., Wang, D., et al. (2023). Hearing of Otof-deficient mice restored by trans-splicing of N- and C-terminal otoferlin. Hum. Genet. *142*, 289–304.
16. Akil, O., Dyka, F., Calvet, C., Emptoz, A., Lahlou, G., Nouaille, S., Boutet de Monvel, J., Hardelin, J.P., Hauswirth, W.W., Avan, P., et al. (2019). Dual AAV-mediated gene therapy restores hearing in a DFNB9 mouse model. Proc. Natl. Acad. Sci. USA *116*, 4496–4501.
17. Al-Moyed, H., Cepeda, A.P., Jung, S., Moser, T., Kügler, S., and Reisinger, E. (2019). A dual-AAV approach restores fast exocytosis and partially rescues auditory function in deaf otoferlin knock-out mice. EMBO Mol. Med. *11*, e9396.
18. Sloan-Heggen, C.M., Bierer, A.O., Shearer, A.E., Kolbe, D.L., Nishimura, C.J., Frees, K.L., Ephraim, S.S., Shibata, S.B., Booth, K.T., Campbell, C.A., et al. (2016). Comprehensive genetic testing in the clinical evaluation of 1119 patients with hearing loss. Hum. Genet. *135*, 441–450.
19. Rodríguez-Ballesteros, M., Reynoso, R., Olarte, M., Villamar, M., Morera, C., Santarelli, R., Arslan, E., Medá, C., Curet, C., Völter, C., et al. (2008). A multicenter study on the prevalence and spectrum of mutations in the otoferlin gene (OTOF) in subjects with nonsyndromic hearing impairment and auditory neuropathy. Hum. Mutat. *29*, 823–831.
20. Iwasa, Y.I., Nishio, S.Y., Sugaya, A., Kataoka, Y., Kanda, Y., Taniguchi, M., Nagai, K., Naito, Y., Ikezono, T., Horie, R., et al. (2019). OTOF mutation analysis with massively parallel DNA sequencing in 2,265 Japanese sensorineural hearing loss patients. PLoS One *14*, e0215932.
21. Choi, B.Y., Ahmed, Z.M., Riazuddin, S., Bhinder, M.A., Shahzad, M., Husnain, T., Riazuddin, S., Griffith, A.J., and Friedman, T.B. (2009). Identities and frequencies

of mutations of the otoferlin gene (OTOF) causing DFNB9 deafness in Pakistan. Clin. Genet. *75*, 237–243.

22. Vona, B., Rad, A., and Reisinger, E. (2020). The Many Faces of DFNB9: Relating OTOF Variants to Hearing Impairment. Genes *11*, 1411.
23. Stalmann, U., Franke, A.J., Al-Moyed, H., Strenzke, N., and Reisinger, E. (2021). Otoferlin Is Required for Proper Synapse Maturation and for Maintenance of Inner and Outer Hair Cells in Mouse Models for DFNB9. Front. Cell. Neurosci. *15*, 677543.
24. Yasunaga, S., Grati, M., Chardenoux, S., Smith, T.N., Friedman, T.B., Lalwani, A.K., Wilcox, E.R., and Petit, C. (2000). OTOF encodes multiple long and short isoforms: Genetic evidence that the long ones underlie recessive deafness DFNB9. Am. J. Hum. Genet. *67*, 591–600.
25. Roux, I., Safieddine, S., Nouvian, R., Grati, M., Simmler, M.C., Bahloul, A., Perfettini, I., Le Gall, M., Rostaing, P., Hamard, G., et al. (2006). Otoferlin, defective in a human deafness form, is essential for exocytosis at the auditory ribbon synapse. Cell *127*, 277–289.
26. Johnson, C. (2011). Otoferlin is a calcium sensor that directly regulates SNARE-mediated membrane fusion. Mol. Biol. Cell *22*.
27. Palazzi, X., Pardo, I.D., Sirivelu, M.P., Newman, L., Kumpf, S.W., Qian, J., Franks, T., Lopes, S., Liu, J., Monarski, L., et al. (2022). Biodistribution and Tolerability of AAV-PHP.B-CBh-SMN1 in Wistar Han Rats and Cynomolgus Macaques Reveal Different Toxicologic Profiles. Hum. Gene Ther. *33*, 175–187.
28. Watakabe, A., Ohtsuka, M., Kinoshita, M., Takaji, M., Isa, K., Mizukami, H., Ozawa, K., Isa, T., and Yamamori, T. (2015). Comparative analyses of adeno-associated viral vector serotypes 1, 2, 5, 8 and 9 in marmoset, mouse and macaque cerebral cortex. Neurosci. Res. *93*, 144–157.
29. Mingozzi, F., Meulenberg, J.J., Hui, D.J., Basner-Tschakarjan, E., Hasbrouck, N.C., Edmonson, S.A., Hutnick, N.A., Betts, M.R., Kastelein, J.J., Stroes, E.S., and High, K.A. (2009). AAV-1-mediated gene transfer to skeletal muscle in humans results in dose-dependent activation of capsid-specific T cells. Blood *114*, 2077–2086.
30. Greenberg, B., Yaroshinsky, A., Zsebo, K.M., Butler, J., Felker, G.M., Voors, A.A., Rudy, J.J., Wagner, K., and Hajjar, R.J. (2014). Design of a phase 2b trial of intracoronary administration of AAV1/SERCA2a in patients with advanced heart failure: the CUPID 2 trial (calcium up-regulation by percutaneous administration of gene therapy in cardiac disease phase 2b). JACC. Heart Fail. *2*, 84–92.
31. Stroes, E.S., Nierman, M.C., Meulenberg, J.J., Franssen, R., Twisk, J., Henny, C.P., Maas, M.M., Zwinderman, A.H., Ross, C., Aronica, E., et al. (2008). Intramuscular administration of AAV1-lipoprotein lipase S447X lowers triglycerides in lipoprotein lipase-deficient patients. Arterioscler. Thromb. Vasc. Biol. *28*, 2303–2304.
32. Greenberg, B., Butler, J., Felker, G.M., Ponikowski, P., Voors, A.A., Desai, A.S., Barnard, D., Bouchard, A., Jaski, B., Lyon, A.R., et al. (2016). Calcium upregulation by percutaneous administration of gene therapy in patients with cardiac disease (CUPID 2): a randomised, multinational, double-blind, placebo-controlled, phase 2b trial. Lancet *387*, 1178–1186.
33. Priddy, F.H., Lewis, D.J.M., and Gelderblom, H.C. (2019). Correction to Lancet HIV 2019; 6: e230-39. Lancet Hiv *6*, e815.
34. Shu, Y., Tao, Y., Wang, Z., Tang, Y., Li, H., Dai, P., Gao, G., and Chen, Z.Y. (2016). Identification of Adeno-Associated Viral Vectors That Target Neonatal and Adult Mammalian Inner Ear Cell Subtypes. Hum. Gene Ther. *27*, 687–699.
35. Askew, C., Rochat, C., Pan, B., Asai, Y., Ahmed, H., Child, E., Schneider, B.L., Aebischer, P., and Holt, J.R. (2015). Tmc gene therapy restores auditory function in deaf mice. Sci. Transl. Med. *7*, 295ra108.
36. Akil, O., Seal, R.P., Burke, K., Wang, C., Alemi, A., During, M., Edwards, R.H., and Lustig, L.R. (2012). Restoration of Hearing in the VGLUT3 Knockout Mouse Using Virally Mediated Gene Therapy. Neuron *75*, 283–293.
37. Chamberlain, K., Riyad, J.M., and Weber, T. (2016). Expressing Transgenes That Exceed the Packaging Capacity of Adeno-Associated Virus Capsids. Hum Gene Ther Method *27*, 1–12.
38. Yan, Z., Zhang, Y., Duan, D., and Engelhardt, J.F. (2000). Trans-splicing vectors expand the utility of adeno-associated virus for gene therapy. Proc. Natl. Acad. Sci. USA *97*, 6716–6721.
39. Trapani, I., Colella, P., Sommella, A., Iodice, C., Cesi, G., de Simone, S., Marrocco, E., Rossi, S., Giunti, M., Palfi, A., et al. (2014). Effective delivery of large genes to the retina by dual AAV vectors. EMBO Mol. Med. *6*, 194–211.
40. Reisinger, E. (2020). Dual-AAV delivery of large gene sequences to the inner ear. Hear. Res. *394*, 107857.
41. Ghosh, A., Yue, Y., Lai, Y., and Duan, D. (2008). A hybrid vector system expands adeno-associated viral vector packaging capacity in a transgene-independent manner. Mol. Ther. *16*, 124–130.
42. Andres-Mateos, E., Landegger, L.D., Unzu, C., Phillips, J., Lin, B.M., Dewyer, N.A., Sanmiguel, J., Nicolaou, F., Valero, M.D., Bourdeu, K.I., et al. (2022). Choice of vector and surgical approach enables efficient cochlear gene transfer in nonhuman primate. Nat. Commun. *13*, 1359.
43. Park, H.K., Cho, J.W., Lee, B.S., Park, H., Han, J.S., Yang, M.J., Im, W.J., Park, D.Y., Kim, W.J., Han, S.C., and Kim, Y.B. (2016). Reference values of clinical pathology parameters in cynomolgus monkeys (Macaca fascicularis) used in preclinical studies. Lab. Anim. Res. *32*, 79–86.
44. Bennett, J., Ashtari, M., Wellman, J., Marshall, K.A., Cyckowski, L.L., Chung, D.C., McCague, S., Pierce, E.A., Chen, Y., Bennicelli, J.L., et al. (2012). AAV2 gene therapy readministration in three adults with congenital blindness. Sci. Transl. Med. *4*, 120ra15.
45. Jacobson, S.G., Cideciyan, A.V., Roman, A.J., Sumaroka, A., Schwartz, S.B., Heon, E., and Hauswirth, W.W. (2015). Improvement and decline in vision with gene therapy in childhood blindness. N. Engl. J. Med. *372*, 1920–1926.
46. Manno, C.S., Pierce, G.F., Arruda, V.R., Glader, B., Ragni, M., Rasko, J.J., Ozelo, M.C., Hoots, K., Blatt, P., Konkle, B., et al. (2006). Successful transduction of liver in hemophilia by AAV-Factor IX and limitations imposed by the host immune response. Nat. Med. *12*, 342–347.
47. Nathwani, A.C., Tuddenham, E.G.D., Rangarajan, S., Rosales, C., McIntosh, J., Linch, D.C., Chowdary, P., Riddell, A., Pie, A.J., Harrington, C., et al. (2011). Adenovirus-associated virus vector-mediated gene transfer in hemophilia B. N. Engl. J. Med. *365*, 2357–2365.
48. Kaplitt, M.G., Feigin, A., Tang, C., Fitzsimons, H.L., Mattis, P., Lawlor, P.A., Bland, R.J., Young, D., Strybing, K., Eidelberg, D., and During, M.J. (2007). Safety and tolerability of gene therapy with an adeno-associated virus (AAV) borne GAD gene for Parkinson's disease: an open label, phase I trial. Lancet *369*, 2097–2105.
49. Zhang, X., He, T., Chai, Z., Samulski, R.J., and Li, C. (2018). Blood-brain barrier shuttle peptides enhance AAV transduction in the brain after systemic administration. Biomaterials *176*, 71–83.
50. Salt, A.N., and Hirose, K. (2018). Communication pathways to and from the inner ear and their contributions to drug delivery. Hear. Res. *362*, 25–37.
51. Landegger, L.D., Pan, B., Askew, C., Wassmer, S.J., Gluck, S.D., Galvin, A., Taylor, R., Forge, A., Stankovic, K.M., Holt, J.R., and Vandenberghe, L.H. (2017). A synthetic AAV vector enables safe and efficient gene transfer to the mammalian inner ear. Nat. Biotechnol. *35*, 280–284.
52. Nist-Lund, C.A., Pan, B., Patterson, A., Asai, Y., Chen, T., Zhou, W., Zhu, H., Romero, S., Resnik, J., Polley, D.B., et al. (2019). Improved TMC1 gene therapy restores hearing and balance in mice with genetic inner ear disorders. Nat. Commun. *10*, 236.
53. Tinling, S.P., and Chole, R.A. (1994). Apical cochlear nerve exposed to perilymph in the gerbil and rat. Hear. Res. *73*, 203–208.
54. Stöver, T., Yagi, M., and Raphael, Y. (2000). Transduction of the contralateral ear after adenovirus-mediated cochlear gene transfer. Gene Ther. *7*, 377–383.
55. Zhang, X.L., Pang, W., Hu, X.T., Li, J.L., Yao, Y.G., and Zheng, Y.T. (2014). Experimental primates and non-human primate (NHP) models of human diseases in China: current status and progress. Dongwuxue Yanjiu *35*, 447–464.
56. Ivanchenko, M.V., Hanlon, K.S., Hathaway, D.M., Klein, A.J., Peters, C.W., Li, Y., Tamvakologos, P.I., Nammour, J., Maguire, C.A., and Corey, D.P. (2021). AAV-S: A versatile capsid variant for transduction of mouse and primate inner ear. Mol. Ther. Methods Clin. Dev. *21*, 382–398.
57. Shinohara, Y., Konno, A., Nitta, K., Matsuzaki, Y., Yasui, H., Suwa, J., Hiromura, K., and Hirai, H. (2019). Effects of Neutralizing Antibody Production on AAV-PHP.B-Mediated Transduction of the Mouse Central Nervous System. Mol. Neurobiol. *56*, 4203–4214.

58. Ranum, P.T., Tecedor, L., Keiser, M.S., Chen, Y.H., Leib, D.E., Liu, X., and Davidson, B.L. (2023). Cochlear transduction via cerebrospinal fluid delivery of AAV in non-human primates. Mol. Ther. *31*, 609–612.

59. Lempert, J., Meltzer, P.E., Wever, E.G., Lawrence, M., and Rambo, J.H.T. (1952). Structure and Function of the Cochlear Aqueduct. AMA. Arch. Otolaryngol. *55*, 134–145.

60. Włodyka, J. (1978). Studies on cochlear aqueduct patency. Ann. Otol. Rhinol. Laryngol. *87*, 22–28.

61. Gopen, Q., Rosowski, J.J., and Merchant, S.N. (1997). Anatomy of the normal human cochlear aqueduct with functional implications. Hear. Res. *107*, 9–22.

62. Bachor, E., Byahatti, S., and Karmody, C.S. (1997). The cochlear aqueduct in pediatric temporal bones. Eur. Arch. Otorhinolaryngol. *254* (*Suppl 1*), S34–S38.

63. Rask-Andersen, H., Tylstedt, S., Kinnefors, A., and Schrott-Fischer, A. (1997). Nerve fibre interaction with large ganglion cells in the human spiral ganglion. A TEM study. Auris Nasus Larynx *24*, 1–11.

64. Jiang, P., Ma, X., Han, S., Ma, L., Ai, J., Wu, L., Zhang, Y., Xiao, H., Tian, M., Tao, W.A., et al. (2022). Characterization of the microRNA transcriptomes and proteomics of cochlear tissue-derived small extracellular vesicles from mice of different ages after birth. Cell. Mol. Life Sci. *79*, 154.

65. Yoshimura, H., Shibata, S.B., Ranum, P.T., and Smith, R.J.H. (2018). Enhanced viral-mediated cochlear gene delivery in adult mice by combining canal fenestration with round window membrane inoculation. Sci. Rep. *8*, 2980.

66. Omichi, R., Yoshimura, H., Shibata, S.B., Vandenberghe, L.H., and Smith, R.J.H. (2020). Hair Cell Transduction Efficiency of Single- and Dual-AAV Serotypes in Adult Murine Cochleae. Mol. Ther. Methods Clin. Dev. *17*, 1167–1177.

67. Chien, W.W., McDougald, D.S., Roy, S., Fitzgerald, T.S., and Cunningham, L.L. (2015). Cochlear gene transfer mediated by adeno-associated virus: Comparison of two surgical approaches. Laryngoscope *125*, 2557–2564.

68. Jiang, L., Wang, D., He, Y., and Shu, Y. (2023). Advances in gene therapy hold promise for treating hereditary hearing loss. Mol. Ther. *31*, 934–950.

69. Zhao, Y., Zhang, L., Wang, D., Chen, B., and Shu, Y. (2022). Approaches and Vectors for Efficient Cochlear Gene Transfer in Adult Mouse Models. Biomolecules *13*, 38.

70. Gu, X., Wang, D., Xu, Z., Wang, J., Guo, L., Chai, R., Li, G., Shu, Y., and Li, H. (2021). Prevention of acquired sensorineural hearing loss in mice by in vivo Htra2 gene editing. Genome Biol. *22*, 86.

71. O'Leary, T.P., Robertson, A., Chipman, P.H., Rafuse, V.F., and Brown, R.E. (2018). Motor function deficits in the 12 month-old female 5xFAD mouse model of Alzheimer's disease. Behav. Brain Res. *337*, 256–263.

72. O'Leary, T.P., Mantolino, H.M., Stover, K.R., and Brown, R.E. (2020). Age-related deterioration of motor function in male and female 5xFAD mice from 3 to 16 months of age. Genes Brain Behav. *19*, e12538.

73. O'Leary, T.P., Gunn, R.K., and Brown, R.E. (2013). What are we measuring when we test strain differences in anxiety in mice? Behav. Genet. *43*, 34–50.

74. Kraeuter, A.K., Guest, P.C., and Sarnyai, Z. (2019). The Y-Maze for Assessment of Spatial Working and Reference Memory in Mice. Methods Mol. Biol. *1916*, 105–111.